# Alkyl Chain Length Effects on Copolymerization Kinetics of a Monoacrylate with Hexanediol Diacrylate

Peter M. Johnson,[†] Jeffrey W. Stansbury,[†,‡] and Christopher N. Bowman*[,†]

*Department of Chemical and Biological Engineering, University of Colorado at Boulder, Boulder, Colorado 80309-0424, and University of Colorado Health Sciences Center, School of Dentistry, Biomaterial Research Center, Aurora, Colorado 80045-0508*

*Received July 10, 2007*

Copolymerizations of hexanediol diacrylate with three monoacrylates were analyzed using high-throughput conversion analysis to elucidate the effects of varying alkyl pendant groups at different compositions. Each analyzed copolymerization system contained hexanediol diacrylate (HDDA), and copolymerizations with 30–60 wt % monoacrylate reached nearly complete conversion after 30 s of exposure time. For higher amounts of monoacrylate, the photopolymerization kinetics of the hexyl acrylate (HA) copolymerization were significantly slower than the copolymerization with either ethylhexyl acrylate (EHA) or dodecyl acrylate (DDA). With 20 wt % HDDA, conversion at 30 s with a comonomer of HA was 62 ± 3%, as compared to 76 ± 3% and 84 ± 3% when copolymerized with EHA and DDA, respectively. Model kinetic parameters were estimated for all four monomer systems, with HDDA monomer parameters found to be within the same error when estimated from any of the copolymerizations. With kinetic parameters for each monomer, comparison maps showing the difference in conversion between two copolymerizations were generated. These comparison maps allow for an assessment of two comonomer systems to determine the optimal photopolymerization conditions. Slower photopolymerization kinetics for HA occur at nearly all compositions containing monoacrylate, with the largest reduction occurring between 20 and 40 wt % monoacrylate.

## Introduction

The modeling of photopolymerization behavior has been a difficult kinetic reaction pathway to predict correctly due to the complexities involved in the polymerization. In the case of radical photopolymerization, generation of the radical species occurs when the initiator generates a radical following absorption of ultraviolet or visible light. Once the radicals are formed, complex and rapidly changing kinetic conditions occur throughout the polymerization. High molecular weight chains and the formation of a cross-linked polymer will begin to impede the termination of radicals; however, monomer diffusion rates remain rapid, leading to an increase in the polymerization rate, or autoacceleration. When the polymerization reaches an even higher double bond conversion, the monomer mobility is also restricted and this restriction leads to a rapid decrease in polymerization as a function of conversion, or autodeceleration. This combination of effects makes photopolymerization difficult to study and model accurately, but the variety of polymer chemistries that are available for photopolymerization and the advantages associated with the photopolymerization process have found practical utility in a wide range of applications such as dental restoratives, coatings, and photoresists.[1–4]

These complex kinetic conditions have been modeled by various groups trying to account for the physiochemical aspects of photopolymerization kinetics. One of the early theories proposed to explain free radical polymerization kinetics began with research performed on styrene polymerizations by Marten and Hamielec,[5] who used a kinetic model to predict diffusion-controlled kinetics. This model was used to simulate the formation of linear polymers but failed to predict cross-linked systems accurately as reaction diffusion-controlled termination was not incorporated. Later work coupling diffusion-controlled kinetics with volume relaxation was conducted by Bowman and Peppas, and it was a better predictor for cross-linked photopolymerization systems.[6] Additional research has expanded on the free volume theory, including adding reaction diffusion termination, using summed reaction resistances, incorporating mass and heat transfer effects, including chain-length-dependent termination, and accounting for oxygen inhibition.[7–13]

The copolymerization model used in this work is an extension of the previous methodology, and it allows for an optimization of kinetic parameters required for the free volume theory. High-throughput conversion analysis allows for the rapid collection of conversion as function of composition and exposure time data which is then used to estimate kinetic parameters for the monomers used in the study.[14,15] The estimation of these parameters is difficult to perform over a wide variety of monomers because the experimentation required to produce all the relevant parameters is complex and necessitates extensive sets of experiments.[16,17] Therefore, this work removes a large portion of

* Author to whom correspondence should be sent. E-mail: Christopher.bowman@colorado.edu.
[†] University of Colorado at Boulder.
[‡] University of Colorado Health Sciences Center.

10.1021/cc700110p CCC: $37.00 
Published on Web 10/26/2007

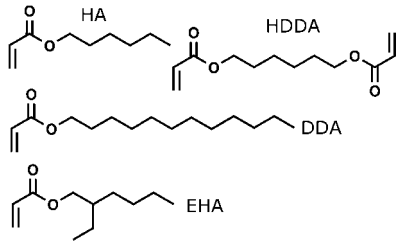


**Figure 1.** Monomers used in this study. Hexanediol diacrylate (HDDA) is copolymerized with each of the three monoacrylates used in this study. Hexyl acrylate (HA), 2-ethyl hexyl acrylate (EHA), and dodecyl acrylate (DDA) vary in the structure and length of the alkyl chain attached to the acrylate group.

the additional parameters required to analyze the data at the cost of somewhat reduced accuracy.

High-throughput techniques were first applied in the material science field to increase the speed of analysis, searching hundreds of unique metallic semiconductors within a short time frame. This approach spread to other fields, including chemistry, biology, and material science. In the field of polymer sciences, high-throughput techniques were first used on polymer–polymer blends annealed to a surface, yielding information on phase behavior as a function of temperature and polymer composition. Other techniques and analytical methods have been developed for surface energy measurements, adhesion, and biocompatibility. However, most of these analyses still use copolymer blends produced from solvated polymers, not monomer composition gradients. Previous work from our group details the analysis of conversion using exposure time and monomer composition gradients.[18] In this paper, the high-throughput technique of analyzing composition and exposure time for photopolymers is applied to three comonomer compositional systems, using a common diacrylate with three separate monoacrylates of varying chain length. These systems are then optimized to find kinetic parameters and compared to show the effects of increasing alkyl chain length on copolymerization kinetics.

## Experimental Section

**Materials.** Hexyl acrylate (HA), 2-ethylhexyl acrylate (EHA), dodecyl acrylate (DDA), and hexanediol diacrylate (HDDA) were obtained from Aldrich (Milwaukee, WI). The photoinitiator dimethoxyphenyl acetophenone (DMPA) was obtained from Ciba-Geigy (Hawthorn, NY). All purchased reagents were used without further purification. Monomer structures are shown in Figure 1.

**Exposure Time and Composition Gradients.** The methodology for exposure time and composition gradients was explained in detail elsewhere, but a brief overview of each gradient is described here.[18] Composition gradients are produced using a small microfluidic mixer with control of the composition dependent on the monomer flow rates. This composition gradient is generated and deposited onto a NaCl salt crystal substrate which is then spread orthogonally across the substrate through shearing the second salt crystal over the gradient. This produces a laminated sample, producing a nearly constant laminate thickness and limiting potential oxygen exposure to the amount dissolved into the monomer solution. Analyzed samples confirm no statistical difference in composition orthogonal to the composition gradient.

To create a gradient of exposure time, a cover plate attached to a linear motion stage is positioned above the sample substrate, with the edge of the cover plate parallel to the composition gradient. When the ultraviolet light (Novacure, 100 W Hg short arc lamp, EXFO, Mississaugua, ON, Canada) is turned on, the cover plate is moved over the sample at a predetermined speed, progressively preventing light from irradiating the substrate and producing an exposure time gradient. The exposure gradient is therefore generated orthogonal to the composition gradient, and preparation of the sample substrate is complete and ready to analyze. The exposure time for each position is determined from the speed of the plate and the region of unexposed distance on the sample, both of which are known during the high-throughput analysis.

**High-Throughput Conversion Analysis.** The methodology to analyze the gradient sample has been explained previously, but briefly, the sample is placed in a Fourier transform infrared (FTIR) microscope (Nicolet Continuum) after both gradients have been generated on the sample.[19] FTIR spectra were measured at 4 $cm^{-1}$ resolution at 4 spectrum scans per point using the IR microscope. A rectangular grid of points is placed on the sample; each of these points is sampled sequentially by the microsope. A grid of 234 points takes 45 min to complete. This analysis corresponds to 9 composition rows with 26 exposure time columns per sample substrate. The microscope aperture is a 100 $\mu$m square, with an aperture variation of 0.3 s in the time direction and a maximum of 0.5 wt % in the composition gradient direction. The positions of the edges of the sample and each grid point are known, allowing for exposure time to be calculated for each IR data point taken. Compositions are determined from IR spectra to ensure the orthogonality of the gradients, with a standard error of 3.1, 3.8, and 3.3% for HA–HDDA, EHA–HDDA, and DDA–HDDA compositions, respectively.

## Copolymerization Kinetic Modeling

The copolymerization model is analyzed in a different system described elsewhere, and an overview of the model and optimization process is described here briefly.[20] This model builds upon the previous modeling approach presented in detail by Goodner and Bowman, explaining free volume dependent modeling for the kinetic parameters.[7] The model has been modified to predict copolymerization of multiple reactive species, in comparison to single monomer kinetic analysis. The model also has been designed to allow for optimization of kinetic model parameters, while simultaneously limiting the number of parameters to fit. Since all model parameters modify either the propagation or termination constant, a large number of parameters will confound and produce unsupported results. Therefore, only reaction diffusion termination and critical free volume resistances are included within the optimization. Free volume is calculated from the free volume of the individual components, using a volume average over all significant components. The set of

equations used to describe the overall free volume in terms of species concentration is:

$$c_{Pi} = c_{Mi0} - c_{Mi} \quad (1)$$

$$v_T = \sum_{i=1}^{n} \left( \frac{c_{Mi} M_{Mi}}{\rho_{Mi}} + \frac{c_{Pi} M_{Mi}}{\rho_{Pi}} \right) \quad (2)$$

$$\varphi_{Mi} = \frac{c_{Mi} M_{Mi}}{\rho_{Mi} v_T} \quad (3)$$

$$\varphi_{Pi} = \frac{c_{Pi} M_{Mi}}{\rho_{Pi} v_T} \quad (4)$$

$$f = 0.025 + \sum_{i=1}^{n} \phi_{Mi} \alpha_{Mi} (T - T_{GMi}) + \phi_P \alpha_P (T - T_{GP}) \quad (5)$$

In these equations, the concentration of monomer, $c_{Mi}$, volume fraction of each monomer, $\phi_{Mi}$, the molecular weight, $M_{Mi}$, and monomer density, $\rho_{Mi}$ are all known or calculated parameters for monomer $i$. The initial concentration of monomer, $c_{Mi0}$, is used to determine the concentration of polymer, with the density of that polymer fraction, $\rho_{Mi}$. The parameter $v_t$ is a normalized total volume used to ensure that volume fractions, $\phi$, sum to unity due to the changes in density with conversion. Coefficients of thermal expansion for the monomer and polymer are $\alpha_{Mi}$ and $\alpha_P$, respectively, and the glass transition temperature of the monomer is denoted as $T_{GMi}$. The polymer volume fractions are combined into a single fraction, with a single polymer glass transition temperature, $T_{GP}$, estimated using the weight fraction of monomer and individual polymer glass transition temperatures. The free volume calculation in eq 5 assumes that free volumes for each component are added ideally thermodynamically and that free volume varies linearly with temperature.[21] This approximation is appropriate for the monomers used here, particularly in light of the need not to introduce additional fitting parameters.

The propagation and termination kinetic constants used in this work include Arrhenius temperature dependence, with resistances by free volume and reaction diffusion kinetics. These kinetic parameters are given in eqs 6 and 7, respectively.

$$k_p = k_{p0} \exp(-E/R_{gas}T)(1 + \exp(A_p(1/f - 1/f_{cp})))^{-1} \quad (6)$$

$$k_t = k_{t0} \exp(-E/R_{gas}T)\left(1 + \frac{1}{Rk_p[M_{tot}]/(k_{t0} \exp(-E/RT)) + \exp(A_t(1/f - 1/f_{ct}))}\right)^{-1} \quad (7)$$

$k_{p0}$ is the pre-exponential kinetic factor for the true reaction kinetic constant for the chemical reaction of radical propagation through unreacted carbon–carbon double bonds of the same monomer type. Similarly, $k_{t0}$ is the pre-exponential kinetic constant for the bimolecular termination reaction of two radicals. $E_{A_p}$ and $E_{A_t}$ are the Arrhenius-based activation energies for propagation and termination, respectively. The term $f$ is the fractional free volume of the polymerizing solution calculated in eq 5; $f_{cp}$ and $f_{ct}$ are the critical fractional free volumes where propagation and termination transition to diffusion control. $A_p$ and $A_t$ govern the rate at which the propagation and termination kinetic parameters decrease as the polymerization becomes diffusion-controlled, and $R$ is the reaction diffusion parameter. $M_{tot}$ is the concentration of any unreacted double bonds, and $R_{gas}$ is the gas constant. This model expands on previous work by allowing the incorporation of any number of monomers for copolymerization. With the addition of multiple monomer and radical species, the number of possible events that could occur expands dependent on both the radical and monomer type. Dissolved oxygen, Z, is also included in the model and the peroxy radicals formed are assumed to be inert over the time span of the model. Since the samples are laminated, dissolved oxygen is not replenished due to diffusion.

**Table 1.** Parameters Used in the Particle Swarm Optimization in All Three Cases

| particle swarm optimization parameter | value |
|---|---|
| $c_1$, $c_2$ | 0.5 |
| $w$ | 0.7 |
| number of particles | 96 |
| range of particle distribution | [0.8 1.2] of initial values |

$$I + h\nu \xrightarrow{R_i} 2R\bullet \quad (8.1)$$

$$R\bullet + M_i \xrightarrow{k_i} P_i\bullet \quad (8.2)$$

$$P_i\bullet + M_j \xrightarrow{k_{p_{ij}}} P_j\bullet \quad (8.3)$$

$$P_i\bullet + P_j\bullet \xrightarrow{k_{t_{ij}}} P_{ij} \quad (8.4)$$

$$P_i\bullet + Z \xrightarrow{k_z} P_iZ \quad (8.5)$$

In this reaction mechanism, eq 8.1 is the photolysis of the initiator, which produces two primary radicals, which are assumed to be of equivalent reactivity in this work. The rate of initiator consumption is determined by the absorption of light and is given by the following equation:

$$R_i = 2\phi \frac{-2.303 \varepsilon C_I I}{E'} \quad (9)$$

where $\varepsilon$ is the molar absorptivity of the initiator, $C_I$ is the photoinitiator concentration, $\phi$ is the product of the efficiency and quantum yield, and $I$ is the light intensity in milliwatts per square centimeter. $E'$ is the energy per mole of photons and is dependent on the wavelength of the illumination source. This value converts the power density given by $I$ into a molar rate for the decomposition of initiator. In this equation, the factor 2 arises since, in most photocleaving initiators, two radicals are produced per initiator molecule.

The second step, shown in eq 8.2, is the chain initiation process. In this reaction, a primary radical reacts with a monomer of type $i$ ($M_i$) to form a polymer chain ($P_i\bullet$) where the reaction rate is determined by the kinetic constant for chain initiation, $k_i$. In this model, $k_i$ is equivalent to a primary radical reaction with any monomer unit. The propagation reactions are represented by eq 8.3, with the kinetic constant of propagation represented as $k_{p_{ij}}$. With multiple monomers, copolymerization between radicals and monomers of different and the same type may occur. The $ij$ subscript denotes a propagation constant where the radical of type $i$ reacts with a double bond of type $j$ to form a new polymer radical of type $j$. The number of propagation reactions is the square of

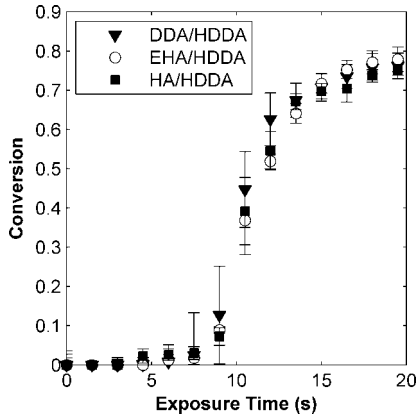


**Figure 2.** HDDA double bond conversion profiles from high-throughput analysis for 100 wt % HDDA from each copolymerization analysis. Samples were polymerized at a light intensity of 3.5 mW/cm$^2$ with 0.5 wt % DMPA at 23 °C using an exposure time gradient of 1.33 mm/s. All three HDDA conversion profiles show results within the standard error of each sample.

the number of polymerizable species in the formulation, as each radical type can polymerize with the same type or any other type of monomer in the system.

Kinetic analysis of propagation in a two-component system requires four values for all conversions, so reactivity ratios are used to simplify the optimization in all multicomponent systems. In a two-component system, reactivity ratios, $r_{12}$ and $r_{21}$, are shown in eqs 10 and 11. Reactivity ratios are used in copolymerization systems to determine the reactivity of one radical type with a monomer of a different type. With a system that contains more than two monomers, additional $r_{ij}$ values are required and employed.

$$r_{12} = k_{p11}/k_{p12} \tag{10}$$

$$r_{21} = k_{p22}/k_{p21} \tag{11}$$

With the monomers used in this study, the reactivity ratios should be near unity as all three monomers are of identical double bond type (acrylate) and they each lack hydrogen bonding or other monomer backbone chemistry features known to produce systems with high reactivity. Therefore, reactivity ratios are assumed to be constant and equal to one throughout the polymerization. The final step in polymerization is termination, denoted by a kinetic constant $k_{t_{ij}}$. Each radical terminates with any other polymer radical in the system, with subscript *ij* denoting the two contributing species types terminating. If dissimilar radicals are terminating, the arithmetic mean of their termination kinetic constants is used. The termination kinetic constant contains both the free volume resistance and a reaction diffusion resistance, which occurs when the system is at a high conversion and pendant radicals have limited mobility.

The model programming determines each distinct composition that has conversion versus exposure time data and then is modeled for the time points required. The differential equations account for only in situ polymerization, and additional computations are require to determine postexpure polymerization, commonly called dark polymerization, at each time point. Since the sampling technique uses an exposure time gradient, radicals still exist when the light has been removed. No new radicals are generated, but polymerization will continue until the remaining radicals are terminated. This additional polymerization is significant in highly cross-linked systems and is required to model the current high-throughput analysis technique accurately.[8,9] Running additional polymerization differential equations for each exposure time and composition sample point necessitates an excess of computational effort, particularly when the model is optimizing parameters. However, the dark polymerization can readily exceed 10% in certain cases, requiring the incorporation of a model to estimate this additional conversion. Therefore, dark polymerization is determined using a semiempirical formula based on equations for a single monomer under the same conditions. The dark polymerization of a two-monomer, two-radical system cannot be solved analytically, so the system was reduced to a lumped single-radical, single-monomer system to estimate the kinetics in this region. This equation assumes constant values of $k_p$ and $k_t$ over the span of the dark polymerization, since the conversion in most cases is not large enough to effect the free volume and consequently the kinetic parameters. The dark polymerization equation uses lumped parameters for $k_p$ and $k_t$, as shown in eq 12. For single monomer systems, this equation will revert to the correct form for dark polymerization of a single monomer.[9]

$$M_{tot} - M_{tot,0} = \frac{k_{pL} M_{tot}}{2k_{tL}} \ln(2k_{tL} R_0 t + 1) \tag{12}$$

$R_0$ is the sum of both radical concentrations when the light is shut off, while $k_{pL}$ and $k_{tL}$ are the lumped kinetic parameters. These lumped parameters are weighted using the volume fractions of the monomer concentration at that point in time. $M_{tot}$ is the total double bond concentration at $t$, the total time after the light has been shut off. $M_{tot,0}$ is the concentration at the point the light exposure ceases. A majority of the dark polymerization will have occurred by the time the sample is placed for analysis, which means that the only relevant conversion is the conversion at long times. The conversion between the differential equation model and the lumped parameter model at long times differs by a maximum of 10% of the conversion attributed to dark polymerization. Since dark polymerization in these systems rarely exceeds 10% of the total conversion, this error is minor in comparison to the other assumptions included in the model. This difference is most significant during autoacceleration but only covers a small portion of the parameter space since the required conditions occur over a small region of exposure time. Due to the limited number of points involved, a larger deviation would be required to alter the parameter search in a significant manner.

The kinetic model described above was programmed in Matlab with a graphic interface, using an ordinary differential equation solver over the time range required. The solver uses a trapezoidal step solver, which works for stiff sets of equations. This solver is required as the initial distributions of points in the parameter optimization could have parameters leading to stiff equations that will slow the optimization down further. A more rigorous analysis of the solver shows less than 0.1% change in conversion as a function of time as compared to more rigorous solvers.

**Table 2.** Parameters Used for Modeling HDDA, HA, EHA, and DDA, Including Optimized Parameters[a]

| parameter | units | HDDA | HA | EHA | DDA | ref |
|---|---|---|---|---|---|---|
| MW | g/mol | 228 | 156.1 | 184.1 | 240.1 | |
| $\rho_m$ | g/mL | 1.010 | 0.888 | 0.888 | 0.889 | |
| $\rho_p$ | g/mL | 1.29 | 1.03 | 1.03 | 0.984 | Painter and Coleman[29] |
| $T_{gm}$ | K | 278 | 228 | 222 | 213 | from $T_m$ |
| $T_{gp}$ | K | 450 | 245 | 213 | 269 | Van Krevelen[28] |
| $E_{A_p}$ | J/mol | 18230 | 18230 | 18230 | 18230 | Goodner et al.[26] |
| $E_{A_t}$ | J/mol | 2970 | 2970 | 2970 | 2970 | Goodner et al.[26] |
| | | | From Model Optimization | | | |
| $k_{p0}$ | L/mol s | $3.43 \times 10^7$ | $3.32 \times 10^7$ | $3.47 \times 10^7$ | $3.58 \times 10^7$ | |
| $k_{t0}$ | L/mol s | $6.12 \times 10^7$ | $6.62 \times 10^7$ | $6.51 \times 10^7$ | $6.44 \times 10^7$ | |
| $f_{cp}$ | | 0.0205 | 0.0348 | 0.032 | 0.0367 | |
| $f_{ct}$ | | 0.0487 | 0.049 | 0.051 | 0.0522 | |
| $A_p$ | | 1.24 | 0.349 | 0.303 | 0.286 | |
| $A_t$ | | 3.6 | 0.448 | 0.356 | 0.401 | |

| additional constants | units | value | ref |
|---|---|---|---|
| $\alpha_m$ | 1/deg C | 0.0005 | Goodner et al.[26] |
| $\alpha_p$ | 1/deg C | 0.00075 | Goodner et al.[26] |
| $\phi$ | | 0.6 | Goodner et al.[26] |
| $\varepsilon$ | L/mol cm | 150 | Goodner et al.[26] |
| $R$ | L/mol | 4 | Anseth et al.[8] |
| $r_{ij}$ | | 1 | |
| $R_{gas}$ | J/mol K | 8.314 | |
| $k_z$ | L/mol s | $3.2 \times 10^8$ | Goodner et al.[26] |

[a] References denote the source of additional parameters.

**Table 3.** Confidence Intervals on the Kinetic Parameters Analyzed Using the Particle Swarm Optimization Protocol

| | | HDDA | | HA | | EHA | | DDA | |
|---|---|---|---|---|---|---|---|---|---|
| $k_{p0}$ | L/mols | 3.4 | $\times 10^7$,3.5$\times 10^7$ | 3.2 | $\times 10^7$,3.4$\times 10^7$ | 3.4 | $\times 10^7$,3.5$\times 10^7$ | 3.5 | $\times 10^7$,3.7$\times 10^7$ |
| $k_{t0}$ | L/mols | 6.0 | $\times 10^7$,6.4$\times 10^7$ | 6.6 | $\times 10^7$,6.7$\times 10^7$ | 6.4 | $\times 10^7$,6.6$\times 10^7$ | 6.3 | $\times 10^7$,6.5$\times 10^7$ |
| $f_{cp}$ | | 0.020, | 0.021 | 0.034, | 0.035 | 0.032, | 0.033 | 0.0367, | 0.0371 |
| $f_{ct}$ | | 0.048, | 0.050 | 0.048, | 0.051 | 0.050, | 0.0515 | 0.0511, | 0.0521 |
| $A_p$ | | 1.2, | 1.3 | 0.33, | 0.36 | 0.29, | 0.312 | 0.286, | 0.293 |
| $A_t$ | | 3.4, | 3.9 | 0.44, | 0.46 | 0.35, | 0.366 | 0.39, | 0.41 |

The optimization protocol uses a particle swarm optimization procedure, used in a variety of continuous function optimization searches.[22–24] All data points, or particles, are represented as four arrays where $j$ corresponds to the number of dimensions in the parameter space. $X_i = (x_{i1}, x_{i2}, \ldots, x_{ij})$ is the current position of the particle, $P_i = (p_{i1}, p_{i2}, \ldots, p_{ij})$ is the best previous position, and $V_i = (v_{i1}, v_{i2}, \ldots, v_{ij})$ is the velocity of the particle $i$. The best optimized result for each particle is also stored, and the best global position with the lowest optimization value is denoted as $P_g = (p_{g1}, p_{g2}, \ldots, p_{gj})$. The parameters of each particle are used, and the conversion results from the model are compared to the data. The error is calculated and compared to the previous best optimization point for that particle and the global particle. Once $P_g$ and $P_i$ have been determined, new velocities and positions are generated, governed by the following equations:

$$v_{id} = wv_{id} + c_1 \,\text{rand}()(p_{id} - x_{id}) + c_2 \,\text{rand}()(p_{gd} - x_{id}) \quad (13)$$

$$x_{id} = x_{id} + v_{id} \quad (14)$$

where $w$ is a inertial weighting factor that decreases with the number of flights taken, and $c_1$ and $c_2$ are two positive constants. The rand() function is two separate random number generators with a range of [0,1]. Further details of the optimization protocol and code are covered extensively elsewhere, and Table 1 shows the parameters used for the particle swarm optimization procedure in this work.[22,24]

The kinetic parameters for the initial values were determined from a previous analysis of HDDA and HA at a different light intensities for all three systems, with HA parameters used as an initial starting point for all three monoacrylates. Initiation kinetics for DMPA has been well-characterized in previous research and limits the error caused by photoinitiation rates.[25] Once the optimization ends, an error plot is generated to ensure that the error is distributed randomly and to ensure that the model fits the data at a reasonable estimate. If the error is not distributed randomly or the optimized result is a poor fit to the data, the optimization is run again. In the case of HDDA, the parameters were determined for all three systems separately. HA, EHA, and DDA kinetic parameters were found using the copolymerization data with HDDA, using their respective data sets.

## Results

High-throughput analysis of composition gradients containing HDDA with a single monoacrylate were performed to produce the results required for the kinetic parameter search. HDDA is a commonly used diacrylate in monomer formulations, and the three monoacrylates chosen produce a well-defined change in polymer properties as a function of the alkyl substituent. All three data sets showed statistically similar HDDA profiles, as shown in Figure 2. The profiles of all three monomers show significant conversion beginning at the same exposure time point, and the highest observed conversion for all three systems is between 80 and 82%, within error. The model kinetic parameters for HDDA are

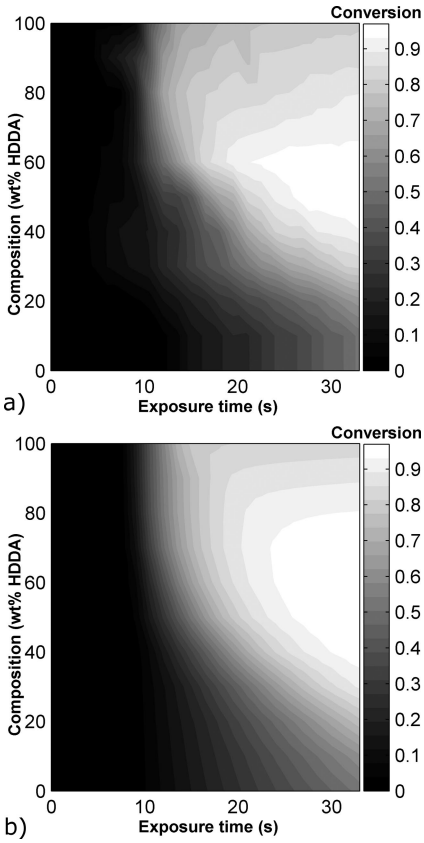


**Figure 3.** HA–HDDA conversion colormap for the high-throughput analysis (a) and the optimized model (b). Samples were polymerized at a light intensity of 3.5 mW/cm$^2$ with 0.5 wt % DMPA at 23 °C using an exposure time gradient of 1.33 mm/s. Modeling was performed at the same conditions, with time and composition points matching all points of the high-throughput data plot.

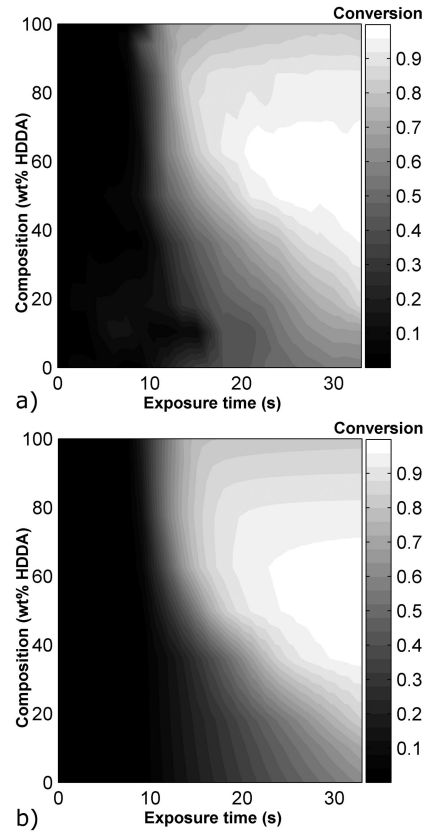


**Figure 4.** EHA–HDDA conversion colormap for the high-throughput analysis (a) and the optimized model (b). Samples were polymerized at a light intensity of 3.5 mW/cm$^2$ with 0.5 wt % DMPA at 23 °C using an exposure time gradient of 1.33 mm/s. Modeling was performed at the same conditions, with time and composition points matching all points of the high-throughput data plot.

the same parameters in all three cases, as expected. The error intervals on the optimized kinetic parameters for HDDA in all three copoylmerizations overlap, showing no statistical difference between the optimization taken in any case. Therefore, an average of these parameters determined from the individual cases was used in the model of all systems. The averaging of these kinetic parameters did not significantly affect the conversion kinetics of any colormap, and increased the average absolute error by less than 0.1%. Table 2 shows the physical properties for each monomer and their optimized kinetic constants used in the copolymerization kinetic model for all four monomers in this study.

**Error Analysis.** The error intervals on the kinetic parameters were determined using the particle swarm tracking parameters, which store every modeled set of kinetic parameters along an associated fit parameter. The particle swarm optimization procedure was done twice, varying six parameters of one monomer while the kinetic parameters of the second monomer remained fixed. This was required as the amount of particles required for an accurate error interval over 12 parameters produced a computationally excessive procedure. An upper limit on the fit parameter was determined using the standard error from the data set, and all points above this limit were discarded. The remaining data set was analyzed to determine the interval on each kinetic parameter. These error intervals are given for each monomer in Table 3.

The parameters derived for this model compare well with data collected from pulsed laser experiments to determine values for $k_p$ for monoacrylates. Alkyl acrylates show $k_p$ kinetic constants at low conversion to lie within a range of 16 000–18 500 L/mol s dependent on the acrylate and the experimental setup.[16,17,27] The predicted model constants lie within this range and also increase with molecular weight. No specific data could be found for hexyl acrylate, but the predicted $k_p$ at low conversion using the model is 15 000 L/mol s, increasing to 19 000 L/mol s for dodecyl acrylate. This range is slightly wider than the range of independently determined propagation constants, but in both cases, the propagation kinetic constant increases with longer alkyl chain length. Data and model results are shown for HA–HDDA in Figure 3, and data and model results are shown for EHA–HDDA in Figure 4. In both cases, similar profiles are seen in both the data and the model, with the EHA–HDDA exhibiting more rapid kinetics for small amounts of HDDA. When compared to the data and model results for DDA–HDDA, which are shown in Figure 5, the trend is even more apparent. This trend is confirmed from the increasing propagation constant with increasing alkyl chain length and reflected in the conversion colormap at a low weight percent of HDDA.

In the HA–HDDA analysis, the maximum error was 15%, with an average absolute error of 4.4%. This error is lower than the previous analysis of HA–HDDA, which had an

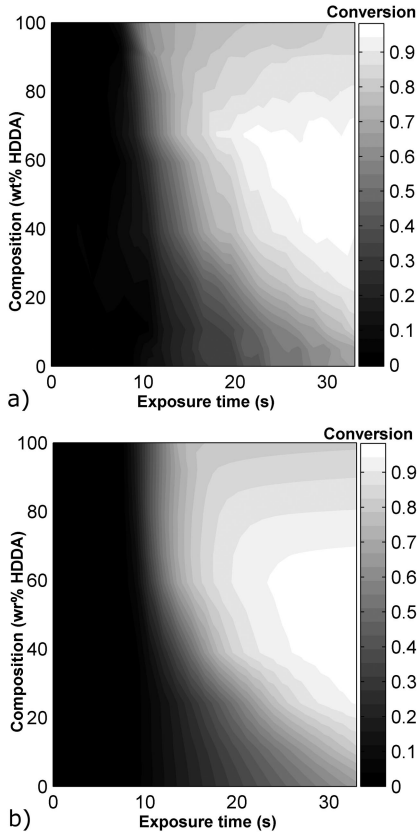


**Figure 5.** DDA–HDDA conversion colormap for the high-throughput analysis (a) and the optimized model (b). Samples were polymerized at a light intensity of 3.5 mW/cm$^2$ with 0.5 wt % DMPA at 23 °C using an exposure time gradient of 1.33 mm/s. Modeling was performed at the same conditions, with time and composition points matching all points of the high-throughput data plot.

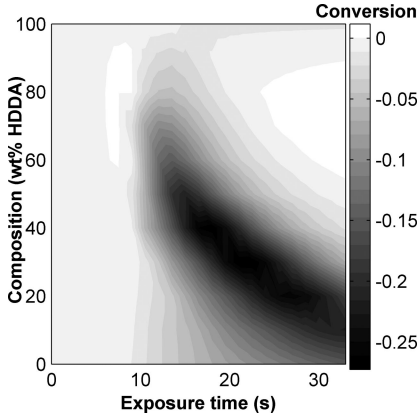


**Figure 6.** Modeled conversion difference of HA–HDDA conversion versus DDA–HDDA conversion model as a function of composition and exposure time. Negative conversion describes a point where an HA–HDDA system has lower conversion than DDA–HDDA at the same time point. Data was modeled at a light intensity of 3.5 mW/cm$^2$ with 0.5 wt % DMPA at 23 °C using an exposure time gradient of 1.33 mm/s.

average absolute error of 5.5%. For the EHA–HDDA and DDA–HDDA copolymerizations, the absolute average error is 3.1 and 3.2% with a maximum error of 26.3 and 23.6%, respectively. In both of these polymerization systems, the largest maximum error is seen near 100 wt % HDDA, due to the fast polymerization rate and the observed data points

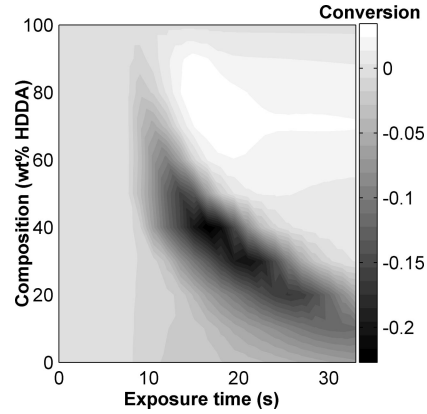


**Figure 7.** Modeled conversion difference of EHA–HDDA conversion versus DDA–HDDA conversion model as a function of composition and exposure time. Negative conversion describes a point where an EHA–HDDA system has lower conversion than DDA–HDDA at the same time point. Data was modeled at a light intensity of 3.5 mW/cm$^2$ with 0.5 wt % DMPA at 23 °C using an exposure time gradient of 1.33 mm/s.

showing a slightly longer inhibition period than predicted by the model. These systems have a lower average error than HA–HDDA from lower error values in compositions near the observed maximum conversion. From the parameter analysis, $k_{p0}$ increases with increasing alkyl chain length, with DDA significantly higher than the other two monoacrylates. Since the activation energies are set equal for all monomers in this analysis, this increase may be caused by either inherently faster polymerization or a reduced activation as compared to EHA or HA. This effect is also seen in pulsed laser experiments, and the change in $k_{p0}$ is required as no combination of $f_{cp}$ and $A_p$ produce a better optimization result.

With all three of the systems modeled, a comparison of conversion at equal conditions was modeled to show better the effect of increasing alkyl chain length on the overall conversion. In Figure 6, the model was used to generate conversion data at constant weight percents of HDDA and either DDA or EHA to compare the kinetics across the entire compositional space. A similar model comparison was performed with HA and DDA, and the results are shown in Figure 7. In both of these cases, HA was used as a baseline conversion, and the conversion colormap from the other copolymerization was subtracted from the HA–HDDA system to produce conversion difference maps. These maps show the difference in conversion between two monomer systems, compared at equal weight percent HDDA.

In Figure 6, the conversion difference map shows a significant region where monomer conversion is decreased when hexyl acrylate is added to the mixture as compared to dodecyl acrylate. This region occurs where there is a significant amount of monoacrylate, and the kinetics of monoacrylate become more important as HDDA requires a significant amount of the monoacrylate to polymerize before autoacceleration occurs. Since HA is slower than DDA as a pure monomer, this behavior delays the onset of significant polymerization and subsequently shows slower kinetics.

A similar region is seen in Figure 7, except the region has expanded in exposure time and composition due to the faster kinetics of DDA as compared to either EHA or HA. However, this comparison also shows that, at higher HDDA

content, the addition of DDA produces a system with less conversion than EHA at later times, since the free volume decreases faster due to a higher polymer glass transition temperature. Since DDA has a higher glass transition temperature than HA, the copolymerization will have a higher polymer glass transition temperature and subsequently lower free volume at equivalent conversion. This effect is also seen in the EHA–HA comparison but is not as significant since there is a smaller difference between EHA and HA kinetic parameters and polymer properties.

## Conclusions

Kinetic parameters were estimated from three copolymerization systems analyzed using high-throughput conversion analysis techniques. All three systems show similar conversion trends as a function of composition and exposure time, with HDDA showing equivalent conversion profiles in all three systems. The three monoacrylates show an increasing trend in conversion with increasing alkyl chain length, which appears in the copolymerization results as well. Using the model, a direct comparison of two copolymerizations was performed, using constant weight percents of HDDA to compare the effect of different monoacrylates over the entire analyzed space. These comparison maps showed two regions with significant conversion change. The first region was with low weight percent HDDA, where the system has reduced autoacceleration, making the photopolymerization kinetic constants of the monoacrylates important. In the second region, at high weight percent HDDA and longer exposure times, HA allows for higher conversion than the other two monoacrylates due to a lower overall glass transition temperature of the polymer and higher monomer mobility as compared to either EHA or DDA.

**Acknowledgment.** We would like to thank the I/UCRC for Fundamentals and Applications of Photopolymerization and the NSF GAANN fellowship for funding.

## References and Notes

(1) Lovell, L. G.; Lu, H.; Elliott, J. E.; Stansbury, J. W.; Bowman, C. N. *Dent. Mater.* **2001**, *17*, 504.
(2) Dickens, S. H.; Stansbury, J. W.; Choi, K. M.; Floyd, C. J. E. *Macromolecules* **2003**, *36*, 6043.
(3) Berchtold, K. A.; Stansbury, J. W.; Bowman, C. N. *J. Dent. Res.* **2000**, *79*, 147.
(4) Khatri, C. A.; Stansbury, J. W.; Schultheisz, C. R.; Antonucci, J. M. *Dent. Mater.* **2003**, *19*, 584.
(5) Marten, F. L.; Hamielec, A. E. *J. Appl. Polym. Sci.* **1982**, *27*, 489.
(6) Bowman, C. N.; Peppas, N. A. *Macromolecules* **1991**, *24*, 1914.
(7) Goodner, M. D.; Newman, S. M.; Bowman, C. N. *J. Dent. Res.* **1995**, *74*, 229.
(8) Anseth, K. S.; Decker, C.; Bowman, C. N. *Macromolecules* **1995**, *28*, 4040.
(9) Anseth, K. S.; Kline, L. M.; Walker, T. A.; Anderson, K. J.; Bowman, C. N. *Macromolecules* **1995**, *28*, 2491.
(10) Anseth, K. S.; Wang, C. M.; Bowman, C. N. *Polymer* **1994**, *35*, 3243.
(11) Lovestead, T. M.; Burdick, J. A.; Ansetha, K. S.; Bowman, C. N. *Polymer* **2005**, *46*, 6226.
(12) Berchtold, K. A.; Lovestead, T. M.; Bowman, C. N. *Macromolecules* **2002**, *35*, 7968.
(13) Lovestead, T. M.; O'Brien, A. K.; Bowman, C. N. *J. Photochem. Photobiol., A: Chem.* **2003**, *159*, 135.
(14) Kurdikar, D. L.; Peppas, N. A. *Macromolecules* **1994**, *27*, 4084.
(15) Kurdikar, D. L.; Peppas, N. A. *Polymer* **1994**, *35*, 1004.
(16) Asua, J. M.; Beuermann, S.; Buback, M.; Castignolles, P.; Charleux, B.; Gilbert, R. G.; Hutchinson, R. A.; Leiza, J. R.; Nikitin, A. N.; Vairon, J. P.; van Herk, A. M. *Macromol. Chem. Phys.* **2004**, *205*, 2151.
(17) Beuermann, S.; Buback, M. *Progr. Polym. Sci.* **2002**, *27*, 191.
(18) Johnson, P. M.; Reynolds, T. B.; Stansbury, J. W.; Bowman, C. N. *Polymer* **2005**, *46*, 3300.
(19) Anseth, K. S.; Bowman, C. N.; Brannon-Peppas, L. *Biomaterials* **1996**, *17*, 1647.
(20) Johnson, P. M.; Bowman, C. N.; Stanbury, J. W. *Macromolecules* **2007**, submitted for publication.
(21) Zhu, S.; Tian, Y.; Hamielec, A. E.; Eaton, D. R. *Polymer* **1990**, *31*, 1726.
(22) Li, X. D. Better Spread and Convergence: Particle Swarm Multiobjective Optimization Using the Maximum Fitness Function. *Proceedings of Genetic and Evolutionary Computation–Gecco*, Seatle, WA, June 26, 2004; Part 1, Vol. 3102, p 117.
(23) Parsopoulos, K. E.; Vrahatis, M. N. *IEEE Trans. Evol. Comput.* **2004**, *8*, 211.
(24) Bo, Z. An Improved Particle Swarm Optimization Algorithm for Global Numerical Optimization. *Proceedings of Computational Science–ICCS*, Reading, UK, May 28, 2006; Part 1, Vol. 3991, p 657.
(25) Goodner, M. D.; Bowman, C. N. *Macromolecules* **1999**, *32*, 6552.
(26) Goodner, M. D.; Lee, H. R.; Bowman, C. N. *Ind. Eng. Chem. Res.* **1997**, *36*, 1247.
(27) Buback, M.; Degener, B.; Huckestein, B. *Makromol. Chem.: Rapid Commun.* **1989**, *10*, 311.
(28) Van Krevelen, D. W. *Properties of Polymers: their correlation with chemial structure, their numerical estimation and prediction from additive group contribution*, 3rd ed.; Elsevier: New York, 1994, pp. 196–200.
(29) Coleman, M. M.; Serman, C. J.; Bhagwaghar, D. E.; Painter, P. C. *Polymer* **1990**, *31*, 1187.

CC700110P